Available online www.jocpr.com

Journal of Chemical and Pharmaceutical Research, 2016, 8(1):236-244

Research Article

ISSN : 0975-7384
CODEN(USA) : JCPRC5

Evaluation of bactericidal activity of reduced graphene oxide supported titania nanoparticles under visible light irradiation

D. Maruthamani*, D. Divakar, M. Harshavardhan and M. Kumaravel

Department of Chemistry, PSG College of Technology, Coimbatore, India

---

ABSTRACT

A series of reduced graphene oxide supported TiO_2 (RGOT) nanocomposites with different weight ratio of carbon content was prepared by a simple one pot solvothermal process using TiO_2 nanoparticles (P-25) and GO as precursors. The as-prepared samples were characterized using various analytical techniques. Furthermore, the antibacterial activity of RGOT-20 nanocomposite was studied and found to be higher in comparison to bare TiO_2 photocatalyst against the bacterial model P.aeruginosa under visible light. Coupling TiO_2 with RGO resulted in a higher photocurrent density and more charge carriers to form reactive species (OH°, O_2°$^-$) promoting the photo-damaging of the cell membrane of the bacteria. The enhanced charge transfer/separation process resulting from the hybrid RGOT nanocomposite is due to the charge transfer interaction between TiO_2 and RGO and it is well supported by the PL and EIS spectra. Studies on the influence of inorganic ions such as HCO_3^-, Cl^-, SO_4^{2-} and NO_3^- were also investigated on the antibacterial property of the nanocomposite.

Keywords: Bactericidal activity, photocatalyst, solvothermal process, graphene, nanocomposite.

INTRODUCTION

Microbial pollutants are the most important next to organic chemicals which degrade the quality of natural waters. Wastewaters may contain bacterial pathogens such as *Salmonella spp., Vibrio spp., Escherichia coli and Shigella spp.*, which are able to cause waterborne diseases such as typhoid, cholera and diarrhea [1]. Disinfection is the last and most important step in water and wastewater treatment process which plays an important role in the control of pathogens and microbial species in water, and can prevent waterborne epidemics and the spread of infectious disease [2, 3]. The most common disinfectants comprise of chlorine, chloramines, ozone, chlorine dioxide, and chlorine gas [4]. These substances release harmful by-products during the course of action, most of them are considered as possible carcinogens, mutagens and teratogens [2, 5]. Furthermore, the resistance of microorganisms to these common chemical disinfectants is increasing; therefore it is essential to develop an ideal disinfectant.

Inorganic semiconductor photocatalysts mediated water disinfection process is the most suitable and environmentally benign process among the various methods of disinfection, which is gaining importance lately [6, 7]. Photocatalytic antibacterial activity is the process inwhich the inactivation of microbes is achieved by a photoactive material. In the photocatalytic disinfection process, the reactive oxygen species generated attack the bacteria and damage their cell membrane [8, 9]. Among the various semiconductor photocatalysts, titanium dioxide has proved itself to be the most suitable material for treating wastewater and industrial effluents because of its biological and chemical inertness, strong oxidizing power, non-toxicity, and long-term stability against photo and chemical corrosion [10]. It has become the most important photocatalyst in environmental bio-decontamination for a large variety of organisms, bacteria, viruses, fungi and cancer cells, which can be totally destroyed and converted to CO_2, H_2O and harmless inorganic anions. Yet there are few drawbacks in TiO_2, such as quick recombination of photoinduced electron-hole pairs and its low photoresponse towards visible light. These two inherent drawbacks make it an undesirable candidate for effective photocatalysis. Therefore numerous approaches were attempted to

improve the charge transport in TiO_2 based catalysts such as noble metal loading, metal ion doping, non-metal doping, dye sensitization and also addition of sacrificial reagents (electron donors or hole scavengers). It has been proposed that functionalization of photocatalyst using graphene and its derivatives could be an alternate way to reduce the associated toxicity of dopants [1, 11].

In the present investigation, we evaluated the enhanced bactericidal activity of the synthesized photocatalysts under visible light towards the mineralization of the bacterial model *Pseudomonas aeruginosa* in aqueous phase. Furthermore, the influences of concentration of catalyst and the inorganic ions on the photocatalytic antibacterial property of the hybrid photocatalysts were also studied.

EXPERIMENTAL SECTION

Commercial P25-TiO_2 (80% anatase, 20% rutile; Brunaure-Emmett-Teller (BET) area, 54.77 m^2/g) procured from Degussa Corporation, Germany was used for all studies and also as a the reference. Natural graphite flakes was purchased from Sigma Aldrich while other chemicals such as sulphuric acid, hydrochloric acid, potassium permanganate, hydrogen peroxide, potassium bromate, potassium persulphate, potassium sulphate, sodium bicarbonate, sodium nitrate, sodium chloride, sodium carbonate, methanol and ethanol were of analytical grade obtained from Merck (India) and used as such without further purification. Double distilled water was used in the catalyst preparation and subsequent catalytic tests.

Synthesis of RGO supported TiO_2 Composites

Firstly, Graphene oxide was prepared following the modified Hummer's method [12]. Reduced graphene oxide supported TiO_2 (RGOT) nanocomposite photocatalyst with varying amounts of RGO (10%, 20%, and 25%) were synthesized through a solvothermal process by adding a definite quantity of GO (0.2 g, 0.4 g and 0.5 g for 10%, 20% and 25% RGO respectively) to 2 g of TiO_2. In a typical process, required amount of GO was sonicated in 50 mL methanol for 30 min at room temperature to achieve uniform dispersions and TiO_2 powder was added to it slowly. The mixture was further stirred mechanically for an hour to ensure complete mixing, and the resulting homogeneous suspension was transferred to a teflon-lined stainless steel autoclave and placed in a hot air oven at 120°C for 8 h. During this process, autogenous pressure generated in the vessel facilitates the reduction of GO to RGO and simultaneously merge TiO_2 onto the RGO layers [13, 14]. The resulting sample was washed repeatedly with water, filtered, dried in vacuum at 60°C and stored in a desiccator until further use. The as-prepared samples were labeled as RGOT-10, RGOT-20 and RGOT-25 respectively.

Characterization of the Catalyst samples

Fourier transform infrared (FT-IR) spectra were recorded in transmission mode on Shimadzu DR-8101A spectrophotometer after pelleting with KBr. Information about the morphology and crystallography of the catalysts were obtained from transmission electron microscopy and selected area electron diffraction (SAED) analysis using (Hitachi JEOL-2010 HRTEM) at an accelerating voltage of 200 kV by depositing aqueous solution of samples onto microgrid to ascertain their morphology and composition. XPS analysis was carried using an Omicron Nanotechnology XPS system with a monochromatic Al Kα radiation (hυ = 1486.6 eV) of source voltage 15 kV and emission current of 20 mA from the region of the binding energy of 100-1000 eV to study the chemical states of Ti, O and C species and the interaction of graphene with TiO_2 in RGOT composite. Photoluminescence (PL) spectra were recorded (Shimadzu RF-5301PC) at room temperature with 325 nm wavelength incident laser light.

Photocatalytic antibacterial Studies

The primary aim of the study is to assess the antibacterial activities of the as-prepared photocatalysts against *P.aeruginosa*. The bacterial strains were received from the Department of Microbiology, PSG College of Arts and Science, Coimbatore, India. Before the experiment, all the apparatus used were autoclaved at 120°C for 15 min to ensure sterility. The bacterial strain was grown at a pH of 7.0 in a Luria-Bertani (LB) medium at 37°C for 24 h containing 5 g of yeast extract, 10 g of tryptone and 5 g of NaCl in 1 L of deionized water [15]. Bacterial cells were then collected by centrifugation followed by multiple washing cycles. After decanting the supernatant, the bacterial cells were re-suspended in sterile water to achieve the desired initial concentrations. The *P.aeruginosa* stock solution of approximately 1×10^5 to 1×10^6 colony forming units per mL (cfu/mL) was then prepared for the anti-bacterial study.

The experiments were conducted at three levels; the first test was to explore the antimicrobial properties of all the synthesized materials namely RGOT-10, RGOT-20, RGOT-25 nanocomposite and bare TiO_2. The second part of the test was to further find out the most effective concentration of the most optimal antibacterial material described in the first experiment. Finally, the interference from major inorganic species in natural water such as HCO_3^-, Cl^-, SO_4^{2-} and NO_3^- on the antibacterial property of the best material was examined by introducing appropriate amounts

of $NaHCO_3$, $NaNO_3$, Na_2SO_4 and NaCl into the suspension. All the experiments were carried out in a photocatalyst slurry system through control samples equipped with a 450 W xenon lamp and a shaker, maintained at room temperature. The reactions were carried out in 100 mL Erlenmeyer flasks placed at a distance of approximately 18 cm from the lamp. In the photocatalytic test, 99 parts by volume of photocatalyst suspension with a concentration of 1 g/mL and 0.5 parts by volume of microbial suspension were used [16]. Before each experiment the catalyst suspensions were freshly prepared in ultrapure water and dispersed into bacterial suspension through ultrasonification (20 min). To investigate the toxicity of the catalysts, the separate experiments were carried out in the absence of light. The effect of light in the disinfection process was determined through photolysis reaction. For this purpose, the photocatalytic disinfection was done in the absence of the catalysts under visible light irradiation. The reaction mixture was maintained at 150 rpm. During the photocatalytic disinfection, 100 µL of the reaction solution was taken out at various intervals and immediately diluted thrice with sterilized water. The diluted sample was spread on nutrient agar and incubated at 37°C for 24 h. The number of colonies formed was counted to determine the number of viable cells. All the above experiments were conducted in triplicates to compensate the biological error. The following equation was used to represent antibacterial activity,

$$\text{Antibacterial rate} = \left(\frac{N_t}{N_0}\right) X\ 100\% \quad (1)$$

where N_0 and N_t are the viable cells count before and after irradiation, respectively.

RESULTS AND DISCUSSION

FT-IR spectral studies

The FTIR spectrum of GO (Figure 1a) shows well-defined peaks corresponding to oxygen containing functional groups such as carboxylate (C-O) at 1050 cm^{-1}, epoxide (C-O-C) at 1223 cm^{-1}, C–O–H deformation peak at 1380 $cm^{-1}$and C–O stretching of COOH groups at 1700 cm^{-1}. In addition, a sharp peak at 1624 cm^{-1} and a broad band above 3000 cm^{-1} typical for adsorbed water on the hydrophilic GO surface were also observed [17]. FTIR spectrum of TiO_2 is shown in Figure 1(b). The bands at about 3433 $cm^{-1}$and 1627 cm^{-1} are attributed to the stretching vibrations of hydroxyl and adsorbed water molecule [18]. Below 950 cm^{-1}, the characteristic vibrations of the inorganic Ti-O-Ti network in TiO_2 can be seen. All the characteristic peaks of GO and TiO_2 are present in the RGOT composites (Figure 2), in addition an absorption band was observed at 1570 cm^{-1}which is attributed to the in-plane vibrations of sp^2 hybridized carbons in the graphene sheets, this also confirms the reduction of GO to RGO during solvothermal process. These results imply that TiO_2 can be susceptible to the interaction with the functional groups of RGO in the nanocomposite. When GO was reduced to RGO, all the peaks arising from oxygen containing functionality were substantially reduced, indicating a reduction of the oxygen content in the sample. In addition a new strong absorption band was observed for RGOT's between 500 and 1000 cm^{-1} suggesting a strong chemical interaction between the surface hydroxyl groups of TiO_2 and the functional groups of graphene oxide which is observed in all the three composites irrespective of the RGO content [19].

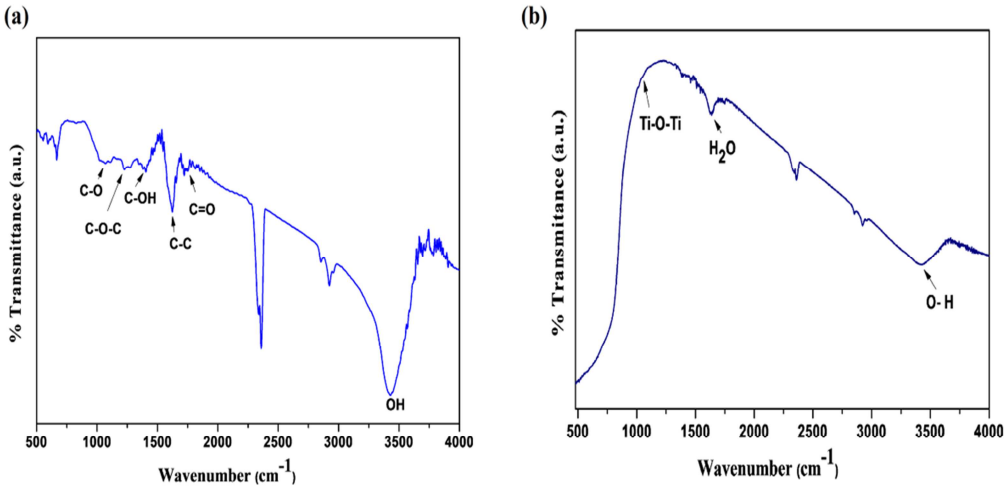

Figure 1: FT-IR spectra of (a) GO, (b) TiO_2

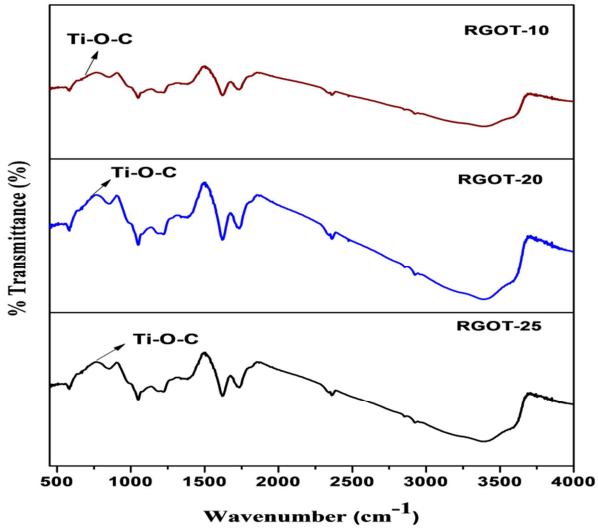

Figure 2: FT-IR spectra of RGOT nanocomposites with various content of RGO

TEM studies

The morphology and structure of RGO nanosheets and RGOT composites were investigated through TEM observation. TEM images of RGO and RGOT-20 nanocomposite are showed in Figure 3 (a,b) The morphology of RGO, consisting of thin stacked flakes and having a well-defined few layer structure at the edges. Figure 3(b) discloses that TiO_2 is dispersed in the RGO matrix and that are eager to accumulate along the wrinkles and edge on the surface of RGO sheets, demonstrating that there is a strong interfacial contact between the graphene sheets and semiconductor TiO_2 matrix. The TiO_2 nanoparticles are not simply mixed up or blended with RGO; rather, they have been entrapped possibly inside the RGO sheets.

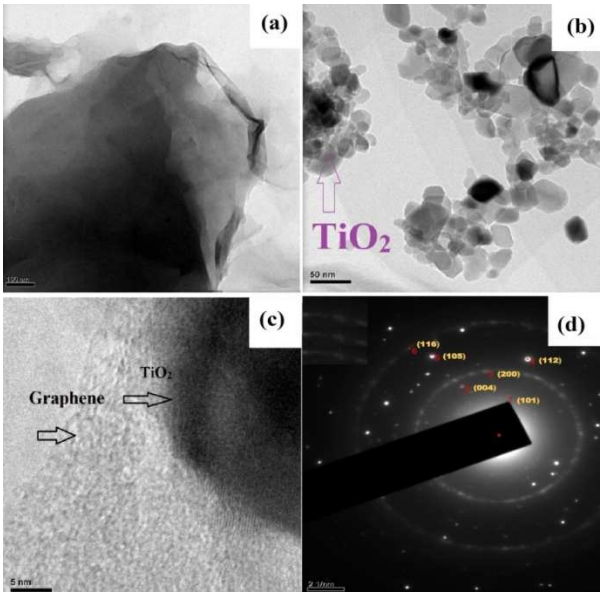

Figure 3: TEM images of (a) RGO, (b) RGOT-20, (c) HRTEM (d) SAED of RGOT-20

HRTEM image of RGOT-20 is shown in Figure 3(c) and the lattice fringes with interplanar distance of 0.362 nm is well observed and which can be assigned to the (101) plane of the TiO_2. SAED pattern clearly shows (Figure 3d) the ring pattern arising from the (101), (004), (105), (116), (112) and (200) plane of anatase TiO_2, further confirming the presence of anatase crystalline structure of the TiO_2 nanoparticles. This structure is favourable for the improvement of the adsorption and photocatalytic property of TiO_2 matrix [10].

XPS spectral studies

The survey spectrum of the RGOT-20 and TiO_2 is shown in Figure 4(a). The survey scan exhibits the presence of main elements namely Ti, C and O. Ti^{4+} ion shows two peaks around binding energy of 458 eV and 464 eV which

are assigned to Ti 2p 3/2 and Ti 2p 1/2 spin respectively, the peaks at binding energies of 530 eV and 285 eV are due to O1s and C1s which was characteristics of oxygen and carbon [20].

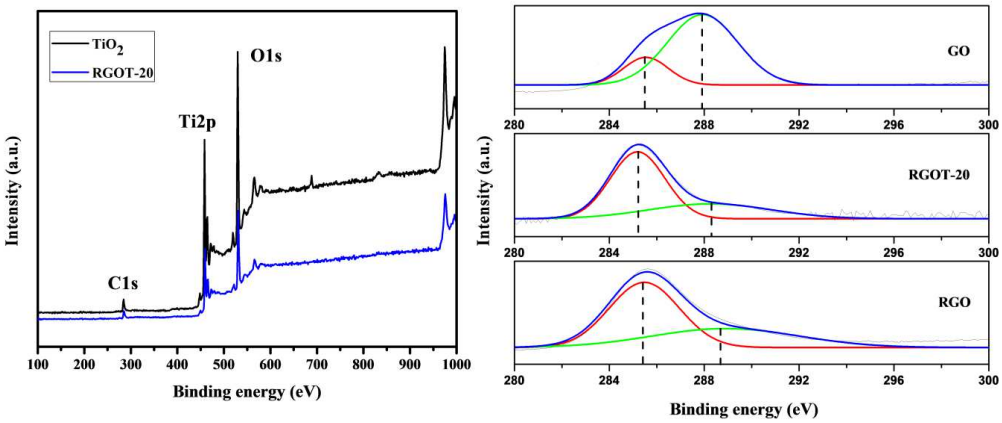

Figure 4: (a) XPS survey scan of TiO_2 and RGOT-20 nanocomposite (b) C 1s spectra of GO, RGO and RGOT-20

XPS spectra of C 1s region for GO, RGO and RGOT-20 are shown in Figure 4(b). The C 1s XPS spectra region can be deconvoluted into two peaks corresponding to two different bonding environments of carbon including C–C (C=C) at 285.5 eV, C–O (hydroxyl and epoxy) or C=O (carboxyl or ketone) at 288.2 ± 0.5 eV. All three samples gave both the peaks; however, we can observe that the C-O content is much greater in GO sample while RGO and RGOT-20 had more C-C linkage than C-O linkage indicating reduction of oxygen functionalities in RGO and RGOT-20 [21, 22].

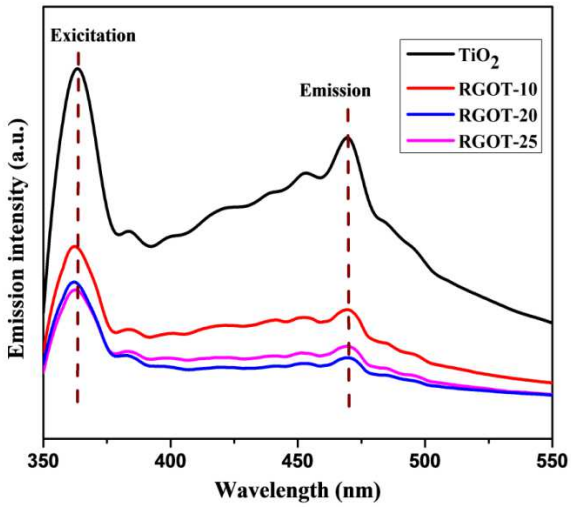

Figure 5: PL spectra of TiO_2 and RGOT nanocomposites with various content of RGO

PL spectral studies

The photoluminescence emission spectroscopy (PL) has been widely used to study the excited state of the photocatalysts and charge transfer behaviour of the photogenerated carriers [23, 24]. Figure 5 illustrates the excitation and emission spectra of TiO_2 and RGOT composite photocatalysts. TiO_2 shows strong emission spectrum at 496 nm with the excitation peak at 362 nm. It was confirmed that the addition of the RGO did not give any influences on the excitation and emission wavelengths but the intensity of the spectra was found to be affected by the presence of RGO which indicates that the recombination rate of photogenerated electron-hole pairs in the composite can be efficiently suppressed by wrapping $TiO_2$with RGO. Since the electron affinity of the TiO_2 is 4.2 eV and the work function of the graphene is known to be 4.42 eV [25], the direct transfer of photoexcited electron from conduction band of TiO_2 to RGO is energetically favourable. This suggests that the presence of RGO might have successfully suppressed the electron-hole recombination of TiO_2. These results further imply that efficient electron transfer is achieved, which is essential for the production of greater amount of hydroxyl radicals. This is particularly important for the semiconductor mediated photocatalytic degradation of pollutants driven by energized electrons [20].

It can be observed that the intensity of the excitation and emission spectra decreased with the increasing loading of RGO from10 to 20 wt%, while higher loading amount of RGO (25wt %) gave a small increment in the intensity than RGOT-20 samples. The higher amount of GO might cause the incident of recombination center at RGO, leading to the slight increase in the intensity of excitation and emission spectra [26].

Bactericidal performances of different Photocatalysts

The photocatalytic inactivation of *P.aeruginosa* by different photocatalysts under visible light irradiation was studied and the results are presented in Figure 6. The photolysis test results reveal that no photolysis of the bacterial cells occurred even after 100 min of visible light irradiation. Furthermore, control experiment result indicated that the RGOT composites showed no toxicity to the bacterial cells as all the cells were active. The bactericidal activity of the reference catalyst (bare TiO_2) was relatively low under visible light irradiation. However, with the addition of the RGO to TiO_2 the photocatalytic disinfection rate increased. It was observed that the bactericidal activities of RGOT-10, RGOT-20 and, RGOT-25, nanocomposites were related to RGO content in the nanocomposites. Noticeably, the RGOT-20 showed better photocatalytic antibacterial activity than RGOT-10. A further increase of RGO content had negative effect on the antimicrobial activity. After 50 min, the bacterial survival rate was in the order: RGOT-20 > RGOT-10 > RGOT-25 > TiO_2 > control > photolysis. This result can be explained as follows: a large number of TiO_2 existed in the RGO; the RGO might be covered by TiO_2 nanoparticles, which could lead to a shield of the active sites of TiO_2 during the antibacterial process [14, 27]. Thus, the samples of RGOT-25 had a lower activity than RGOT-20 and RGOT-10.

The excellent antibacterial activity of RGOT-20 and RGOT-10 could be attributed to the efficient separation of photo-generated electron–hole pairs, since RGO could be used as an electron acceptor and transporter [15,28], suggesting that more °OH is produced due to efficient charge separation and are involved in the antibacterial activity. On the other hand, the RGO and TiO_2 had a synergism of inhibiting survival of the bacteria.

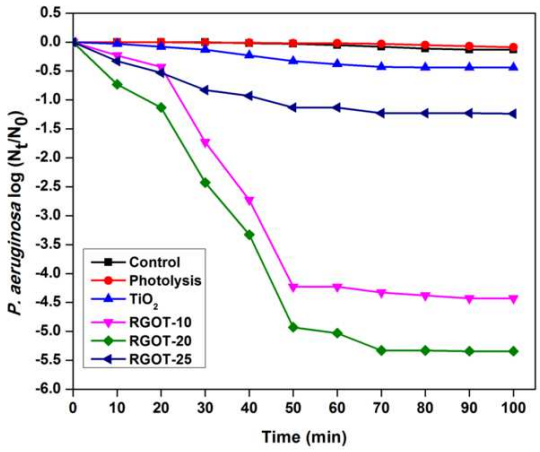

Figure: 6 Photocatalytic bactericidal properties against *P.aeruginosa* on different materials under visible light irradiation [Control: RGOT-20 in dark condition, photolysis: light only, (catalyst concentration: 200 mg/L, initial bacterial concentration: 10^5–10^6 cfu/mL, light intensity: 100 mw/cm^2)]

The potential reason for the enhanced antibacterial rate of RGOT-20 was due to the higher °OH production rate as explained above. To confirm this, ethanol was used as hydroxyl radical scavenger [27, 28]. Experiments were performed using RGOT-20 with different ethanol concentrations namely 0, 25, 50, 75 and 100 mM. Figure 7, indicates that the bacterial survival rate increased with the increase in the ethanol concentration from 0 to 100 mM. This could be explained based on the fact that more ethanol would remove more °OH, and thereby decreases the efficiency of the catalysts towards bacterolysis and thus helps the increased bacterial survival rate. Thus the result suggested that °OH played a significant role in the bacterial inactivation [15, 27, 28].

Influence of concentration of RGOT-20 on disinfection performance

Figure 8, shows the effects of RGOT-20 dosage on photo-disinfection of *P.aeruginosa* under visible light irradiation for 50 min. When the concentration of RGOT-20 was increased from 50 and 150 mg/L, the photolysing rate also increased, at the end of 50 min the bacterial survival rates decreased in the scale of 4log reduction with the concentration of 150 mg/L. This result could be attributed the production of higher amounts of °OH with increasing amounts of RGOT-20 above 150 mg/L. The increase of catalyst dosage retarded the antibacterial rate, which may be due to the agglomeration of the catalyst at higher concentration, which lead to the reduction of the contact between the photocatalyst and bacteria [31]. In addition, the agglomerated catalyst particles coupled with increase in turbidity of the suspension resulted in light scattering and decreased light penetration during the reaction.

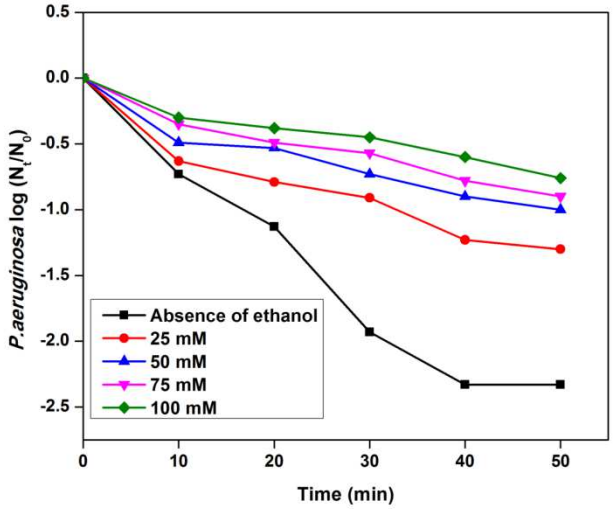

Figure: 7 Effect of ethanol on the antimicrobial properties of RGOT-20 against *P.aeruginosa* [RGOT-20 concentration: 150mg/L, initial bacterial concentration: 10^5–10^6cfu/mL, light intensity: 100 mw/cm^2]

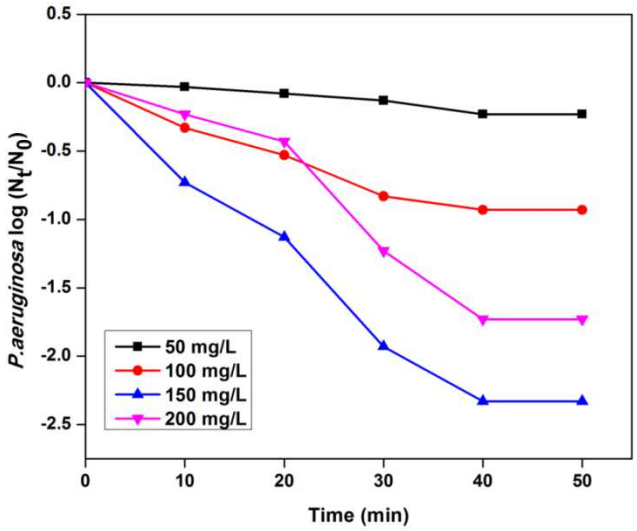

Figure: 8 Influence of RGOT-20 dosage on antimicrobial properties against *P.aeruginosa* under visible light after 50 min exposure time [initial bacteria concentration: 10^5–10^6 cfu/mL, light intensity: 100 mw/cm^2]

Influence of Inorganic ions on Bacterial activity of RGOT-20

The influence of the inorganic ions on the photocatalytic inactivation of the bacterial cells by RGOT-20 was studied and results are presented in Figure 9. All the ions had varying degrees of influence on the antibacterial activity of the RGOT-20 at the same concentration (0.2mM). The bacterial survival rate increased in the presence of bicarbonate ions, due to the capturing of the photo generated holes on the catalyst surface as shown in Equation 2.

$$HCO_3^- + h^+ \rightarrow HCO_3^{\circ -} \quad (2)$$

In addition, bicarbonate ions decreases the concentration of reactive oxygen species (•OH) produced by the catalyst as shown in Equation 3,

$$^\circ OH + HCO_3^- \rightarrow CO_3^{\circ -} + H_2O \quad (3)$$

The presence of SO_4^{2-} and NO_3^- anions inhibits the antibacterial activity of the catalyst by establishing the physical force of attractions such as Van der Waals force and hydrogen bond with TiO_2 [15,32,33]. Compared with HCO_3^-, SO_4^{2-} and NO_3^- anions, Cl^- had a minimum effect on the antibacterial activity of the photocatalyst. Cl^- has the ability to block the photoactive sites of the catalyst and also acts as scavenger of hydroxyl radical as shown in Equation 4 [32]. However, Kang et al [35], pointed that bacterial metabolic process could produce chloride radicals (Cl°), Cl^- could react with Cl° and rapidly get equilibrated with chloride radical anion ($Cl^{\circ -}$) as shown in Equation 5, $Cl^{\circ -}$ also a known disinfectant, therefore, accelerating the bactericidal rate [32, 36].

$$^{\circ}OH + Cl^{-} \rightarrow Cl^{\circ} + OH^{-} \quad (4)$$

$$Cl^{\circ} + Cl^{-} \rightarrow Cl^{\circ -} \quad (5)$$

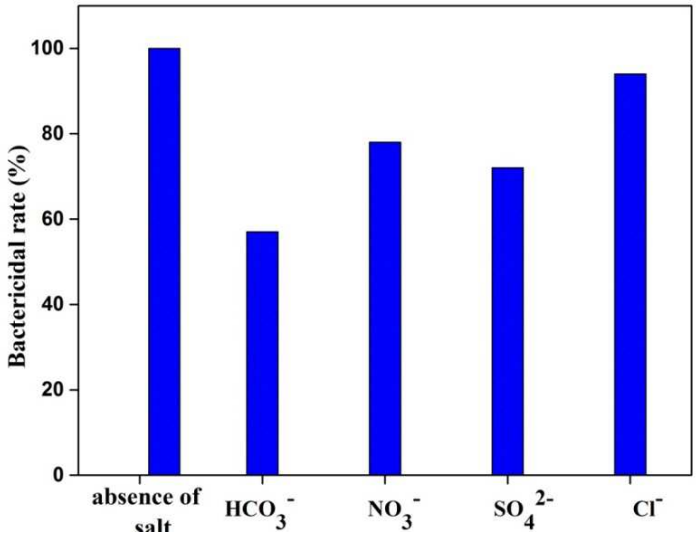

Figure: 9 Influence of inorganic ions against the bactericidal rate of *P.aeruginosa* [concentration of the ions: 0.2 mM, catalyst concentration (RGOT-20): 150 mg/L, initial bacterial concentration: 10^5–10^6 cfu/mL, light intensity: 100 mw/cm^2, irradiation time: 50 min]

CONCLUSION

TEM photographs of the sample confirmed that the surface of the RGO sheets are decorated by a homogeneous dispersion of TiO_2 nanoparticles and that are eager to accumulate along the wrinkles and edge on the surface of RGO sheets, demonstrating that there is a strong interfacial contact between the graphene sheets and semiconductor TiO_2 matrix. Among the catalyst prepared RGOT-20 achieved the most excellent antibacterial property in comparison with bare TiO_2 photocatalyst against the bacterial model *P.aeruginosa*. Dark tests indicated that the RGOT composites showed no toxicity to the *P.aeruginosa* cells. After 50 min visible light irradiation, the bacterial inactivation rate nearly achieved 100% at the most effective concentration of 150 mg/L. The addition of inorganic ions reduced the antibacterial activity of the RGOT-20. The bacterial survival rates in the presence of HCO_3^- decreased the inactivation rates to a larger extent than Cl^-, SO_4^{2-} and NO_3^-. The reason for the activity of the HCO_3^- is that HCO_3^- captured the h^+ produced by TiO_2 and inhibit the generation of reactive oxygen species.

REFERENCES

[1] H Zheng; PC Maness; DM Blake; EJ Wolfrum; SL Smolinski; WA Jacoby. *J. Photochem Photobiol A Chem.*, **2000**, 130(2), 163-170.
[2] Q Li; S Mahendra; DY Lyon; L Brunet; MV Liga; D Li. *Water Res.*, **2008**, 42(18), 4591-4602.
[3] D Gangadharan; K Harshvardan; G Gnanasekar; D Dixit; KM Popat; PS Anand. *Water Res.*, **2010**, 44(18), 5481-5487.
[4] N Savage; MS Diallo. *J. Nanopart Res.*, **2005**, 7(4-5), 331-342.
[5] SD Richardson; MJ Plewa; ED Wagner; R Schoeny; DM DeMarini. *Mutat Res.*, **2007**, 636(1), 178-242.
[6] D Venieri; A Fraggedaki; M Kostadima; E Chatzisymeon; V Binas; A Zachopoulos; G Kiriakidis; D Mantzavinos. *Appl Catal B: Environ.*, **2014**, 154-155, 93-101.
[7] AA Ashkarran; H Hamidinezhad; H Haddadi; M Mahmoudi. *Appl Surf Sci.*, **2014**, 301, 338-345.
[8] Q Bao; D Zhang; P Qi. *J.Colloid Interf Sci.*, **2011**, 360(2), 463-470.
[9] JS Kim; E Kuk; KN Yu; JH Kim, SJ Park; HJ Lee; SH Kim; YK Park; YH Park; CY Hwang; YK Kim; YS Lee; DH Jeong; MH Cho. *Nanomed Nanotechnol.*, **2007,** 3(1), 95-101.
[10] N Raghavan; S Thangavel; G Venugopal. *Mat Sci Semicon Proc.*, **2015**, 30, 321-329.
[11] T Saito; T Iwase; T Morioka. *J. Photochem Photobio A: Chem.*, **1992**, 14(4), 369-379.
[12] P Wang; Y Ao; C Wang; J Hou; J Qian. *J. Hazard Mater.*, **2012**, 223-224, 79-83.
[13] MQ Yang; N Zhang; YJ Xu. *Appl Mater Inter.*, **2013**, 5(3), 1156-1164.
[14] W Fan; Q Lai; Q Zhang; Y Wang. *J. Phys Chem C.*, **2011**, 115(21), 10694-10701.
[15] YN Chang; XM Ou; GM Zeng; JL Gong; CH Deng; Y Jiang; J Liang; GQ Yuan; HY Liu; X He. *Appl Surf Sci.*, **2015**, 343, 1-10.

[16] R Rahimi; S Zargari; A Yousefi; MY Berijani; A Ghaffarinejad; A Morsali. 2015, *Appl Surf Sci.*, **2015**, 355, 1098-1106.
[17] DC Marcano; DV Kosynkin; JM Berlin; A Sinitskii; Z Sun; A Slesarev; LB Alemany; W Lu; JM Tour. *ACS Nano.*, 2010, 4(8), 4806-4814.
[18] Y Si; ET Samulski. *Nano Letters.*, **2008,** 8(6), 1679-1682.
[19] G Wang; J Yang; J Park; X Gou; B Wang; H Liu. *J. Phys Chem C.*, **2008**, 112(22), 8192- 8195.
[20] X Wang; J Wang; X Dong; F Zhang; L Ma; X Fei; X Zhang; H Ma. *J. Alloy Compd.*, **2016**, 656, 181-188.
[21] X Huan; G Li; J Li; C Chen; X Ren. *J.Mol Liq.*, **2016**, 213, 58-68.
[22] S Jiang; R Wang; M Pang; H Wang; S Zeng; X Yue; L Ni; Y Yu; J Dai; S Qiu; Z Zhang. *Electrochem Acta.*, **2015**,182, 406-415.
[23] N Zhang; YH Zhang; YJ Xu. *Nanoscale.*, **2012**, 4(19), 5792-5813.
[24] J Zhu; J He. *Appl Mat Interf.*, **2012**, 4(3), 1770-1776.
[25] J Zhou; J Gao. *J. Hazard Mater.*, **2011**, 185(2-3), 710-716.
[26] NS Alim; HO Lintang; L Yuliati. *Malay J. Fund Appl Sci.*, **2015**, 11(3), 118-121.
[27] B Cao; S Cao; P Dong; J Gao; J Wang. *Materials Letters*, **2013**, 93, 349-352.
[28] P Gao; K Ng; DD Sun. *J. Hazard Mater*, **2013**,262, 826-835.
[29] MV Liga; EL Bryant; VL Colvin; Q Li. *Water Res.*, **2011**, 45(2), 535-544.
[30] M Cho; H Chung; W Choi; Y Yoon. *Appl Environ Microb.*, **2005**, 71(1), 270-275.
[31] C Jayaseelan; AA Rahuman; SM Roopan; AV Kirthi; J Venkatesan; SK Kim; M Iyappan; C Siva. Spectrochim Acta A: Mol Biomol Spectrosc., **2013**, 107, 82-89.
[32] A Rincon. *Appl Catal B: Environ.*, **2004**, 51(4), 283-302.
[33] DM Alrousan; PS Dunlop; TA McMurray; JA Byrne. *Water Res.*,**2009**, 43(1), 47-54.
[34] X Wang; TT Lim. *Water Res.*, **2013**, 47(12), 4148-4158.
[35] MG Kang, HS Jung, KJ Kim. *J. Photochem Photobio: A Chem.*, **2000**, 136(1), 117-123.
[36] S Sontakke; C Mohan; J Modak; G Madras. *Chem Eng J.*, **2012**, 189, 101-107.